

Article

# Frequency Analysis of Asymmetric Circular Organic Solar Cells Embedded in an Elastic Medium under Hygrothermal Conditions

Muneer Alali <sup>1</sup>, Mohammad A. Abazid <sup>1</sup>  and Mohammed Sobhy <sup>1,2,\*</sup> 

<sup>1</sup> Department of Mathematics and Statistics, College of Science, King Faisal University, P.O. Box 400, Al-Ahsa 31982, Saudi Arabia; 220000562@student.kfu.edu.sa (M.A.); mabazid@kfu.edu.sa (M.A.A.)

<sup>2</sup> Department of Mathematics, Faculty of Science, Kafrelsheikh University, Kafrelsheikh 33516, Egypt

\* Correspondence: msobhy@kfu.edu.sa

**Abstract:** This research represents the first theoretical investigation about the vibration behavior of circular organic solar cells. Therefore, the vibration response of asymmetric circular organic solar cells that represent a perfect renewable energy source is demonstrated. For this purpose, the differential quadrature method (DQM) is employed. The organic solar cell is modeled as a laminated plate consisting of five layers of Al, P3HT:PCBM, PEDOT:PSS, ITO, and Glass. This cell is rested on a Winkler–Pasternak elastic foundation and assumed to be exposed to various types of hygrothermal loadings. There are three different kinds of temperature and moisture variations that are taken into account: uniform, linear, and nonlinear distribution throughout the cell’s thickness. The displacement field is presented based on a new inverse hyperbolic shear deformation theory considering only two unknowns. The motion equations including hygrothermal effect and plate–foundation interaction are established within the framework of Hamilton’s principle. The DQM is utilized to solve these equations. In order to ensure the accuracy of the proposed theory, the present results are compared with those reported by other higher-order theories. A comprehensive parametric illustration is conducted on the impacts of different parameters involving the geometrical configuration, elastic foundation parameters, temperature, and moisture concentration on the deduced eigenfrequency of the circular organic solar cells.



check for updates

**Citation:** Alali, M.; Abazid, M.A.; Sobhy, M. Frequency Analysis of Asymmetric Circular Organic Solar Cells Embedded in an Elastic Medium under Hygrothermal Conditions. *Symmetry* **2024**, *16*, 577. <https://doi.org/10.3390/sym16050577>

Academic Editor: Alexei Kanel-Belov

Received: 3 March 2024

Revised: 14 April 2024

Accepted: 18 April 2024

Published: 7 May 2024



**Copyright:** © 2024 by the authors. Licensee MDPI, Basel, Switzerland. This article is an open access article distributed under the terms and conditions of the Creative Commons Attribution (CC BY) license (<https://creativecommons.org/licenses/by/4.0/>).

**Keywords:** differential quadrature method; asymmetric circular organic solar cells; hygrothermal; vibration

## 1. Introduction

It is well known that ample energy is essential for the development process and the global economy and prosperity. The most common classical kind of energy-producing materials are fossil fuels. However, they will eventually run out, may pollute the ecosystem, and increase the fuel global warming. Therefore, moving away from fossil fuels toward renewable energy is very important. Due to its clean, sustainable, and widespread availability, solar energy is becoming the leading contender to address both the energy problem and the global warming. Solar power is a clean, renewable source of energy that forms a sizable amount of the world’s electricity [1]. A special kind of solar cells is the organic solar cells. Their absorbing layers are based on organic semiconductors [2,3]. They have properties such as thinness, ease of production, affordability, and compact structure. Organic solar cells have been used in a variety of industries, including vehicles and airplanes [3]. They have much more energy conversion efficiencies than other classical ones. To guarantee that they operate consistently, organic solar cells must be examined in many conditions, like solar radiation, heat, moisture, and wind. The influences of the solar irradiation and wind speed on the stresses of the organic solar cell were discussed by Liu et al. [4]. Joodaki and Salari [5] utilized low-frequency noise spectroscopy to study the behavior of organic

cells under mechanical deformation. Furthermore, Duc et al. [6] developed an analytical method to examine the nonlinear vibrational behavior of rectangular organic cells exposed to external force. To improve the organization of the carbon black and graphite in the carbon cathode, Zhang et al. [7] used a unique vibration approach which enhanced the contact sites of the perovskite and carbon layer interface of perovskite solar cells. Using AMPS software, Liao et al. [8] performed computation analysis on BaSi<sub>2</sub>-based np or nip homo-junction solar cells with high optical absorption material. Dat et al. [9] analyzed the nonlinear buckling of organic solar cells under axial compressive pressures based on classical plate theory. Van Tuyen [10] illustrated the vibration and buckling of organic nanobeams exposed to thermal load using the nonlocal theory and the sinusoidal shear deformation theory. Liu et al. [11] used the modified couple stress theory and an effective isogeometric analysis method to investigate the size effect on the buckling response of the organic solar cells in thermal environment. Based on various shear strain theories and the nonlocal theory, Tien et al. [12] explained the vibration and bending responses of the organic nanoplates employing Navier procedure and the finite element method.

The fact that organic solar cells are naturally thin and flexible requires utilizing flexibility foundations in their production. This is needed to preserve their structure and functionality when they are exposed to stress or deformation. Therefore, a flexible base must be placed beneath them during the manufacturing process to improve their stability and enable a related simple installation. The elastic foundations are advantageous for supporting organic solar cells. This is because they reduce the stresses and deformations that organic solar cells experience as a result of variations in temperature, pressure, or humidity [13]. Moreover, they improve the quality of organic solar cells and protect them from scuffing during installation. Furthermore, they preserve cell functionality even after bending. Therefore, it is vital to investigate the effects of elastic foundations on the behavior of the solar cells under various conditions. The vibration and static bending of the size-dependent organic solar cell resting on a Winkler–Pasternak elastic foundation were explored by Li et al. [14] utilizing the modified strain gradient theory and a refined shear deformation plate theory. Li et al. [15] employed the classical plate theory and von Karman nonlinearity to analyze the nonlinear dynamic behavior of an organic cell resting on an elastic medium subjected to an external excitation and thermal load. Moreover, the effects of Winkler–Pasternak elastic foundation on the buckling behavior of the organic solar cells were demonstrated by Li et al. [13] utilizing the refined shear deformation plate theory and the modified strain gradient theory. Further, Van Quyen and Duc [16] studied the influences of the elastic foundation, mechanical load, and thermal load on the nonlinear dynamic response and vibration of the organic solar panels employing the Galerkin and Runge–Kutta methods.

There has been a lot of research on the performance of organic solar cells with various shapes under the effects of different conditions as displayed in the previous studies. However, to the best of our knowledge, neither a circle-shaped study nor one under idealized hygrothermal circumstances have been conducted. Therefore, the vibration response of asymmetric circular organic solar cells exposed to various types of hygrothermal loadings is analyzed in our study. Furthermore, the novelty of our work consists in utilization of a new inverse hyperbolic shear deformation theory to describe the displacement field depending only on two unknowns. It is assumed that the organic solar cells are rested on a Winkler–Pasternak elastic foundation to improve their performance. The motion equations are developed from Hamilton's principle and then solved using the differential quadrature method (DQM). A comprehensive parametric illustration is conducted on the impacts of different parameters involving the geometrical configuration, elastic foundation parameters, temperature, and moisture concentration on the deduced eigenfrequency of the circular organic solar cells.

## 2. Refined Plate Theory for Circular Cells

### 2.1. Main Assumptions

The inquiry model used in this work is composed of five distinct material layers, each with the same radius  $R$  and total thickness  $h$ , which are Al, P3HT:PCBM, PEDOT:PSS, ITO, and Glass. Additionally, two elastic foundation layers (Winkler and shear layers) support the cells (see, Figure 1). In the Cartesian coordinate system, Shimpi's plate theory is established based on a number of assumptions [17]. It is clear that the suppositions are also suitable to use in the circular coordinate system  $(r, \theta, z)$  taking into consideration that the components of the displacement field in the  $r$ ,  $\theta$ , and  $z$  directions are  $(U, V, W)$ , respectively. Thus, it follows that [17]

1. Compared to the in-plane stresses  $\sigma_r$  and  $\sigma_\theta$ , the transverse normal stress  $\sigma_z$  is insignificant.
2. Because the displacements are minimal, the strains involved are very small.
3. The shear component  $W^s$  and the bending component  $W^b$  make up the lateral displacement  $W$ .
4. There are two components for the in-plane displacements:
  - (a) Bending components  $U^b$  and  $V^b$  are, respectively, similar to the displacements  $U$  and  $V$  of the classical plate theory. As a result, the expressions of  $U^b$  and  $V^b$  are

$$\begin{aligned} U^b &= -z \frac{\partial W^b}{\partial r}, \\ V^b &= \frac{-z}{r} \frac{\partial W^b}{\partial \theta}. \end{aligned} \quad (1)$$

- (b) Shear stresses  $\tau_{rz}$  and  $\tau_{r\theta}$  are zero at  $z = \pm \frac{h}{2}$  due to the parabolic variations of shear strains  $\gamma_{rz}$  and  $\gamma_{r\theta}$  that are caused by the shear components  $U^s$  and  $V^s$  of the displacements  $U$  and  $V$ .

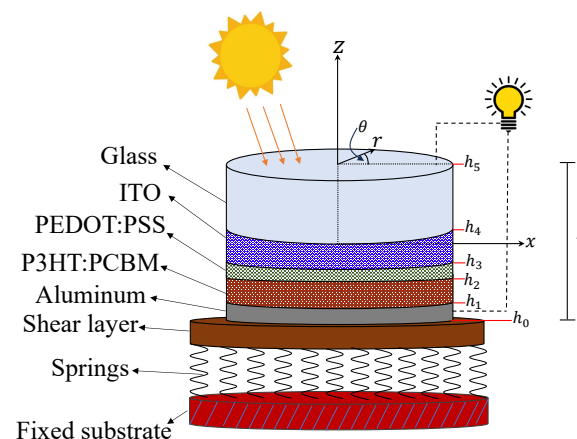


**Figure 1.** A circular organic solar cell on elastic foundations.

### 2.2. Displacement Field

Based on the above assumptions, the displacement field can be expressed as

$$\begin{aligned} U(r, \theta, z, t) &= U^b + U^s = -z \frac{\partial W^b}{\partial r} - f(z) \frac{\partial W^s}{\partial r}, \\ V(r, \theta, z, t) &= V^b + V^s = \frac{-z}{r} \frac{\partial W^b}{\partial \theta} - \frac{f(z)}{r} \frac{\partial W^s}{\partial \theta}, \\ W(r, \theta, z, t) &= W^b(r, \theta, t) + W^s(r, \theta, t), \end{aligned} \quad (2)$$

where  $t$  denotes the time,  $f(z) = z - \hat{f}(z)$ , and

$$\hat{f}(z) = \frac{h}{2} \sinh^{-1}\left(2\frac{z}{h}\right) - \frac{2\sqrt{2}}{3h^2}z^3. \quad (3)$$

For the third-order plate theory (TDPT) [18], sinusoidal plate theory (SDPT) [19], hyperbolic plate theory (HDPT) [20], and exponential plate theory (EDPT) [21], the function  $\hat{f}(z)$  can be given as:

$$\begin{aligned} \hat{f}(z) &= z\left(1 - \frac{4z^2}{3h^2}\right), & \text{for TDPT,} \\ \hat{f}(z) &= \frac{h}{\pi} \sin\left(\frac{\pi z}{h}\right), & \text{for SDPT,} \\ \hat{f}(z) &= h \sinh\left(\frac{z}{h}\right) - z \cosh\left(\frac{1}{2}\right), & \text{for HDPT,} \\ \hat{f}(z) &= z \exp\left(\frac{-2z^2}{h^2}\right), & \text{for EDPT,} \end{aligned} \quad (4)$$

It is evident that the refined plate theory converges to the classical plate theory when  $\hat{f}(z) = 0$ .

### 2.3. Strains and Stresses

The strain field can be calculated as follows:

$$\begin{aligned} e_r &= \frac{\partial U}{\partial r} = -z \frac{\partial^2 W^b}{\partial r^2} - f(z) \frac{\partial^2 W^s}{\partial r^2}, \\ e_\theta &= \frac{1}{r} \left( \frac{\partial V}{\partial \theta} + U \right) = \frac{-z}{r} \left( \frac{\partial W^b}{\partial r} + \frac{1}{r} \frac{\partial^2 W^b}{\partial \theta^2} \right) - \frac{f(z)}{r} \left( \frac{\partial W^s}{\partial r} + \frac{1}{r} \frac{\partial^2 W^s}{\partial \theta^2} \right), \\ e_z &= \frac{\partial W}{\partial z} = 0, \\ \gamma_{r\theta} &= \frac{\partial V}{\partial r} + \frac{\partial U}{r \partial \theta} - \frac{V}{r} = \frac{1}{r} \left( \frac{2z}{r} \frac{\partial W^b}{\partial \theta} + \frac{2f(z)}{r} \frac{\partial W^s}{\partial \theta} - 2z \frac{\partial^2 W^b}{\partial \theta \partial r} - 2f(z) \frac{\partial^2 W^s}{\partial \theta \partial r} \right), \\ \gamma_{rz} &= \frac{\partial U}{\partial z} + \frac{\partial W}{\partial r} = \hat{f}'(z) \frac{\partial W^s}{\partial r}, \quad \hat{f}'(z) = \frac{\partial \hat{f}(z)}{\partial z}, \\ \gamma_{\theta z} &= \frac{\partial V}{\partial z} + \frac{\partial W}{r \partial \theta} = \hat{f}'(z) \frac{\partial W^s}{r \partial \theta}, \end{aligned} \quad (5)$$

where  $e_r$  and  $e_\theta$  are normal strains and  $e_{r\theta} = \frac{1}{2}\gamma_{r\theta}$ ,  $e_{rz} = \frac{1}{2}\gamma_{rz}$ , and  $e_{\theta z} = \frac{1}{2}\gamma_{\theta z}$  are shear strains.

Additionally, the stresses for a circular organic cell may be expressed using constitutive equations that consider the hygrothermal loads as follows:

$$\begin{aligned} \sigma_r^{(m)} &= \frac{E^{(m)}}{(1 - [\nu^{(m)}]^2)} [e_r + \nu^{(m)} e_\theta - (1 + \nu^{(m)}) \alpha^{(m)} T(z) - (1 + \nu^{(m)}) \beta^{(m)} C(z)], \\ \sigma_\theta^{(m)} &= \frac{E^{(m)}}{(1 - [\nu^{(m)}]^2)} [e_\theta + \nu^{(m)} e_r - (1 + \nu^{(m)}) \alpha^{(m)} T(z) - (1 + \nu^{(m)}) \beta^{(m)} C(z)], \\ \sigma_z^{(m)} &= 0, \\ \sigma_{r\theta}^{(m)} &= \frac{E^{(m)}}{1 + \nu^{(m)}} e_{r\theta}, \\ \sigma_{rz}^{(m)} &= \frac{E^{(m)}}{1 + \nu^{(m)}} e_{rz}, \\ \sigma_{\theta z}^{(m)} &= \frac{E^{(m)}}{1 + \nu^{(m)}} e_{\theta z}, \quad m = 1, 2, \dots, 5, \end{aligned} \quad (6)$$

where  $E^{(m)}$  and  $\nu^{(m)}$  are Young's modulus and Poisson's ratio of the  $m$ th layer, respectively.  $\alpha^{(m)}$  stands for the coefficient of thermal expansion, while  $\beta^{(m)}$  denotes the coefficient of moisture expansion.  $T(z)$  and  $C(z)$  denote the applied temperature and moisture, respectively.

#### 2.4. Hygrothermal Field

The following distinct temperature and moisture distributions through the thickness are taken into consideration in the current analysis for a precise description of the temperature and moisture influences:

$$\Theta(z) = \begin{cases} \Delta\Theta, & \text{Uniform;} \\ \Delta\Theta\left(\frac{z}{h} + \frac{1}{2}\right) + \Theta_b, & \text{Linear;} \\ \Delta\Theta\left\{1 - \cos\left[\frac{\pi}{2}\left(\frac{z}{h} + \frac{1}{2}\right)\right]\right\} + \Theta_b, & \text{Nonlinear.} \end{cases} \quad (7)$$

$$\Delta\Theta = \Theta_t - \Theta_b, \quad \Theta = T, C,$$

where  $T_t$  and  $C_t$  stand for the temperature and moisture at the top surface, respectively, while  $T_b$  and  $C_b$  stand for the temperature and moisture at the bottom surface, respectively.

### 3. Governing Equations

Hamilton's principle [22] is applied to derive the governing differential equations; it is expressed as

$$\int_0^t (\delta S + \delta K - \delta W_f) dt = 0, \quad (8)$$

where  $\delta S$ ,  $\delta K$ , and  $\delta W_f$  are, respectively, the strain energy, kinetic energy, and external energy variations, which can be expressed as

$$\delta S = \sum_{m=1}^5 \int_0^{2\pi} \int_0^R \int_{h_{m-1}}^{h_m} (\sigma_r^{(m)} \delta e_r + \sigma_\theta^{(m)} \delta e_\theta + 2\sigma_{r\theta}^{(m)} \delta e_{r\theta} + 2\sigma_{rz}^{(m)} \delta e_{rz} + 2\sigma_{\theta z}^{(m)} \delta e_{\theta z}) r dz dr d\theta, \quad (9)$$

$$\delta K = \sum_{m=1}^5 \int_0^{2\pi} \int_0^R \int_{h_{m-1}}^{h_m} \rho^{(m)} (\ddot{U} \delta U + \dot{V} \delta V + \dot{W} \delta W) r dz dr d\theta, \quad (10)$$

$$\delta W_f = \int_0^{2\pi} \int_0^R (N_0 - R_f) \delta W r dr d\theta, \quad (11)$$

where  $\ddot{\Theta} = \partial^2 \Theta / \partial t^2$ ,  $\rho$  is density and  $(h_1, h_2, h_3, h_4)$  are the coordinates among the layers, while  $h_0 = -h/2$  and  $h_5 = h/2$ . Also,  $N_0$  is the in-plane external force due to the hygrothermal load and  $R_f$  is the foundation reaction per unit area, which is given as

$$R_f = J_1 (W^b + W^s) - J_2 \left( \frac{\partial^2}{\partial r^2} + \frac{1}{r} \frac{\partial}{\partial r} + \frac{1}{r^2} \frac{\partial^2}{\partial \theta^2} \right) (W^b + W^s) \quad (12)$$

$$N_0 = (N^T + N^C) \left( \frac{\partial^2}{\partial r^2} + \frac{1}{r} \frac{\partial}{\partial r} + \frac{1}{r^2} \frac{\partial^2}{\partial \theta^2} \right) (W^b + W^s)$$

in which Winkler's spring stiffness is represented by  $J_1$ , the stiffness of the shear layer is represented by  $J_2$ ,  $N^T$  indicates heat force, and  $N^C$  denotes humidity force. Forces  $N^T$  and  $N^C$  are defined as [23]

$$\begin{aligned}
 N^T &= - \sum_{m=1}^5 \int_{h_{m-1}}^{h_m} \frac{E^{(m)}}{1-\nu^{(m)}} \alpha^{(m)} T(z) dz \\
 N^C &= - \sum_{m=1}^5 \int_{h_{m-1}}^{h_m} \frac{E^{(m)}}{1-\nu^{(m)}} \beta^{(m)} C(z) dz
 \end{aligned} \tag{13}$$

The governing equations can be obtained by inserting Equations (9)–(11) into Equation (8) as

$$\begin{aligned}
 \delta W^b &: \frac{2}{r} \frac{\partial N_r}{\partial r} + \frac{\partial^2 N_r}{\partial r^2} - \frac{\partial N_\theta}{r \partial r} + \frac{1}{r^2} \frac{\partial^2 N_\theta}{\partial \theta^2} + \frac{2}{r^2} \frac{\partial N_{r\theta}}{\partial \theta} + \frac{2}{r} \frac{\partial^2 N_{r\theta}}{\partial \theta \partial r} + I_1 \nabla^2 \ddot{W}^b + I_2 \nabla^2 \ddot{W}^s \\
 &- I_4 (\ddot{W}^b + \ddot{W}^s) + N_0 - R_f = 0, \\
 \delta W^s &: \frac{2}{r} \frac{\partial M_r}{\partial r} + \frac{\partial^2 M_r}{\partial r^2} - \frac{1}{r} \frac{\partial M_\theta}{\partial r} + \frac{1}{r^2} \frac{\partial^2 M_\theta}{\partial \theta^2} + \frac{2}{r^2} \frac{\partial M_{r\theta}}{\partial \theta} + \frac{2}{r} \frac{\partial^2 M_{r\theta}}{\partial \theta \partial r} \\
 &+ \frac{M_{rz}}{r} + \frac{\partial M_{rz}}{\partial r} + \frac{1}{r} \frac{\partial M_{\theta z}}{\partial \theta} + I_2 \nabla^2 \ddot{W}^b + I_3 \nabla^2 \ddot{W}^s - I_4 (\ddot{W}^b + \ddot{W}^s) + N_0 - R_f = 0,
 \end{aligned} \tag{14}$$

where

$$\begin{aligned}
 \{N_r, N_\theta, N_{r\theta}\} &= \sum_{m=1}^5 \int_{h_{m-1}}^{h_m} \{\sigma_r^{(m)}, \sigma_\theta^{(m)}, \sigma_{r\theta}^{(m)}\} z dz, \\
 \{M_r, M_\theta, M_{r\theta}\} &= \sum_{m=1}^5 \int_{h_{m-1}}^{h_m} \{\sigma_r^{(m)}, \sigma_\theta^{(m)}, \sigma_{r\theta}^{(m)}\} f(z) dz, \\
 \{M_{rz}, M_{\theta z}\} &= \sum_{m=1}^5 \int_{h_{m-1}}^{h_m} \{\sigma_{rz}^{(m)}, \sigma_{\theta z}^{(m)}\} \hat{f}(z) dz, \\
 \{I_1, I_2, I_3, I_4\} &= \sum_{m=1}^5 \int_{h_{m-1}}^{h_m} \rho^{(m)} \{z^2, z f(z), f^2(z), 1\} dz.
 \end{aligned} \tag{15}$$

By inserting Equation (6) into Equation (15) with the aid of Equation (5), we obtain

$$\begin{aligned}
 N_r &= -k_1 \frac{\partial^2 W^b}{\partial r^2} - k_2 \frac{\partial^2 W^s}{\partial r^2} - \frac{\bar{k}_1}{r} \left( \frac{\partial W^b}{\partial r} + \frac{1}{r} \frac{\partial^2 W^b}{\partial \theta^2} \right) - \frac{\bar{k}_2}{r} \left( \frac{\partial W^s}{\partial r} + \frac{1}{r} \frac{\partial^2 W^s}{\partial \theta^2} \right) - k_3, \\
 N_\theta &= -\frac{k_1}{r} \left( \frac{\partial W^b}{\partial r} + \frac{1}{r} \frac{\partial^2 W^b}{\partial \theta^2} \right) - \frac{k_2}{r} \left( \frac{\partial W^s}{\partial r} + \frac{1}{r} \frac{\partial^2 W^s}{\partial \theta^2} \right) - \bar{k}_1 \frac{\partial^2 W^b}{\partial r^2} - \bar{k}_2 \frac{\partial^2 W^s}{\partial r^2} - k_3, \\
 N_{r\theta} &= \frac{k_7}{r^2} \frac{\partial W^b}{\partial \theta} + \frac{k_8}{r^2} \frac{\partial W^s}{\partial \theta} - \frac{k_7}{r} \frac{\partial^2 W^b}{\partial \theta \partial r} - \frac{k_8}{r} \frac{\partial^2 W^s}{\partial \theta \partial r}, \\
 M_{rz} &= k_6 \frac{\partial W^s}{\partial r}, \\
 M_{\theta z} &= \frac{k_6}{r} \frac{\partial W^s}{\partial \theta}, \\
 M_r &= -k_2 \frac{\partial^2 W^b}{\partial r^2} - k_4 \frac{\partial^2 W^s}{\partial r^2} - \frac{\bar{k}_2}{r} \left( \frac{\partial W^b}{\partial r} + \frac{1}{r} \frac{\partial^2 W^b}{\partial \theta^2} \right) - \frac{\bar{k}_4}{r} \left( \frac{\partial W^s}{\partial r} + \frac{1}{r} \frac{\partial^2 W^s}{\partial \theta^2} \right) - k_5, \\
 M_\theta &= -\frac{k_2}{r} \left( \frac{\partial W^b}{\partial r} + \frac{1}{r} \frac{\partial^2 W^b}{\partial \theta^2} \right) - \frac{k_4}{r} \left( \frac{\partial W^s}{\partial r} + \frac{1}{r} \frac{\partial^2 W^s}{\partial \theta^2} \right) - \bar{k}_2 \frac{\partial^2 W^b}{\partial r^2} - \bar{k}_4 \frac{\partial^2 W^s}{\partial r^2} - k_5, \\
 M_{r\theta} &= \frac{k_8}{r^2} \frac{\partial W^b}{\partial \theta} + \frac{k_9}{r^2} \frac{\partial W^s}{\partial \theta} - \frac{k_8}{r} \frac{\partial^2 W^b}{\partial \theta \partial r} - \frac{k_9}{r} \frac{\partial^2 W^s}{\partial \theta \partial r},
 \end{aligned} \tag{17}$$

where

$$\begin{aligned}
 \{k_1, k_2, k_4\} &= \sum_{m=1}^5 \int_{h_{m-1}}^{h_m} \frac{E^{(m)}}{1 - [\nu^{(m)}]^2} \{z^2, zf(z), f^2(z)\} dz, \\
 \{\bar{k}_1, \bar{k}_2, \bar{k}_4\} &= \sum_{m=1}^5 \int_{h_{m-1}}^{h_m} \frac{\nu^{(m)} E^{(m)}}{1 - [\nu^{(m)}]^2} \{z^2, zf(z), f^2(z)\} dz, \\
 \{k_3, k_5\} &= \sum_{m=1}^5 \int_{h_{m-1}}^{h_m} \frac{E^{(m)}}{1 - [\nu^{(m)}]^2} \{z, f(z)\} (1 + \nu^{(m)}) (\alpha^{(m)} \Delta T + \beta^{(m)} \Delta C) dz, \\
 \{k_6, k_7, k_8, k_9\} &= \sum_{m=1}^5 \int_{h_{m-1}}^{h_m} \frac{E^{(m)}}{2(1 + \nu^{(m)})} \{[\hat{f}'(z)]^2, 2z^2, 2zf(z), 2f^2(z)\} dz.
 \end{aligned} \tag{18}$$

To establish the governing Equation (14) in terms of the displacement components, we can insert Equations (16) and (17) into Equation (14) to obtain

$$\begin{aligned}
 & -k_1 \frac{\partial^4 W^b}{\partial r^4} - k_2 \frac{\partial^4 W^s}{\partial r^4} - \frac{k_1}{r^4} \frac{\partial^4 W^b}{\partial \theta^4} - \frac{k_2}{r^4} \frac{\partial^4 W^s}{\partial \theta^4} + \left( \frac{-2k_7 - 2\bar{k}_1}{r^2} \right) \frac{\partial^4 W^b}{\partial r^2 \partial \theta^2} \\
 & + \left( \frac{-2k_8 - 2\bar{k}_2}{r^2} \right) \frac{\partial^4 W^s}{\partial r^2 \partial \theta^2} - \frac{2k_1}{r} \frac{\partial^3 W^b}{\partial r^3} - \frac{2k_2}{r} \frac{\partial^3 W^s}{\partial r^3} + \left( \frac{2k_7 - 6\bar{k}_1}{r^3} \right) \frac{\partial^3 W^b}{\partial r \partial \theta^2} \\
 & + \left( \frac{2k_8 - 6\bar{k}_2}{r^3} \right) \frac{\partial^3 W^s}{\partial r \partial \theta^2} + \left( \frac{k_1 - 4\bar{k}_1}{r^2} + N^T + N^C + J_2 \right) \frac{\partial^2 W^b}{r^2} \\
 & + \left( \frac{k_2 - 4\bar{k}_2}{r^2} + N^T + N^C + J_2 \right) \frac{\partial^2 W^s}{r^2} + \left( \frac{-2k_1 - 2\bar{k}_1 - 2k_7}{r^4} + \frac{N^T + N^C + J_2}{r^2} \right) \frac{\partial^2 W^b}{\theta^2} \\
 & + \left( \frac{-2k_2 - 2\bar{k}_2 - 2k_8}{r^4} + \frac{N^T + N^C + J_2}{r^2} \right) \frac{\partial^2 W^s}{\theta^2} + \left( \frac{-k_1}{r^3} + \frac{N^T + N^C + J_2}{r} \right) \frac{\partial W^b}{r} \\
 & \left( \frac{-k_2}{r^3} + \frac{N^T + N^C + J_2}{r} \right) \frac{\partial W^s}{r} + (J_2 - J_1) W^b + (J_2 - J_1) W^s + I_1 \frac{\partial^2 \ddot{W}^b}{\partial r^2} \\
 & + I_2 \frac{\partial^2 \dot{W}^s}{\partial r^2} + \frac{I_1}{r^2} \frac{\partial^2 \ddot{W}^b}{\partial \theta^2} + \frac{I_2}{r^2} \frac{\partial^2 \dot{W}^s}{\partial \theta^2} + \frac{2I_1}{r} \frac{\partial \ddot{W}^b}{\partial r} + \frac{2I_2}{r} \frac{\partial \dot{W}^s}{\partial r} - I_4 \ddot{W}^b - I_4 \dot{W}^s = 0, \\
 & -k_2 \frac{\partial^4 W^b}{\partial r^4} - k_4 \frac{\partial^4 W^s}{\partial r^4} - \frac{k_2}{r^4} \frac{\partial^4 W^b}{\partial \theta^4} - \frac{k_4}{r^4} \frac{\partial^4 W^s}{\partial \theta^4} + \left( \frac{-2k_8 - 2\bar{k}_2}{r^2} \right) \frac{\partial^4 W^b}{\partial r^2 \partial \theta^2} \\
 & + \left( \frac{-2k_9 - 2\bar{k}_4}{r^2} \right) \frac{\partial^4 W^s}{\partial r^2 \partial \theta^2} - \frac{2k_2}{r} \frac{\partial^3 W^b}{\partial r^3} - \frac{2k_4}{r} \frac{\partial^3 W^s}{\partial r^3} + \left( \frac{2k_8 - 6\bar{k}_2}{r^3} \right) \frac{\partial^3 W^b}{\partial r \partial \theta^2} \\
 & + \left( \frac{2k_9 - 6\bar{k}_4}{r^3} \right) \frac{\partial^3 W^s}{\partial r \partial \theta^2} + \left( \frac{k_2 - 4\bar{k}_2}{r^2} + N^T + N^C + J_2 \right) \frac{\partial^2 W^b}{r^2} \\
 & + \left( \frac{k_4 - 4\bar{k}_4}{r^2} + N^T + N^C + J_2 + \frac{k_6}{2} \right) \frac{\partial^2 W^s}{r^2} + \left( \frac{-2k_2 - 2\bar{k}_2 - 2k_8}{r^4} + \frac{N^T + N^C + J_2}{r^2} \right) \frac{\partial^2 W^b}{\theta^2} \\
 & + \left( \frac{-2k_4 - 2\bar{k}_4 - 2k_9}{r^4} + \frac{N^T + N^C + J_2}{r^2} + \frac{k_6}{2r} \right) \frac{\partial^2 W^s}{\theta^2} + \left( \frac{-k_2}{r^3} + \frac{N^T + N^C + J_2}{r} \right) \frac{\partial W^b}{r} \\
 & \left( \frac{-k_4}{r^3} + \frac{N^T + N^C + J_2 + \frac{k_6}{2}}{r} \right) \frac{\partial W^s}{r} + (J_2 - J_1) W^b + (J_2 - J_1) W^s + I_2 \frac{\partial^2 \ddot{W}^b}{\partial r^2} \\
 & + I_3 \frac{\partial^2 \dot{W}^s}{\partial r^2} + \frac{I_2}{r^2} \frac{\partial^2 \ddot{W}^b}{\partial \theta^2} + \frac{I_3}{r^2} \frac{\partial^2 \dot{W}^s}{\partial \theta^2} + \frac{2I_2}{r} \frac{\partial \ddot{W}^b}{\partial r} + \frac{2I_3}{r} \frac{\partial \dot{W}^s}{\partial r} - I_4 \ddot{W}^b - I_4 \dot{W}^s = 0.
 \end{aligned} \tag{20}$$

The displacements of the circular plate are assumed to be represented by the succeeding trigonometric Fourier series [24]. Therefore, the displacements are given as

$$\begin{aligned} W^b &= \sum_{n=1}^{\infty} u^b(r) \sin(\mu_n \theta) e^{i\omega t}, \\ W^s &= \sum_{n=1}^{\infty} u^s(r) \sin(\mu_n \theta) e^{i\omega t}, \end{aligned} \quad (21)$$

in which  $u^b(r)$  and  $u^s(r)$  are functions in  $r$ ,  $\omega$  is the eigenfrequency,  $i = \sqrt{-1}$  and  $\mu_n = 1, 2, 3, \dots$ .

The governing equations are obtained by substituting the displacements (21) into Equations (19) and (20) as follows:

$$\begin{aligned} &a_1 \frac{d^4 u^b(r)}{dr^4} + a_2 \frac{d^4 u^s(r)}{dr^4} + \frac{a_3}{r} \frac{d^3 u^b(r)}{dr^3} + \frac{a_4}{r} \frac{d^3 u^s(r)}{dr^3} + \left(a_5 + \frac{a_6}{r^2}\right) \frac{d^2 u^b(r)}{dr^2} \\ &+ \left(a_7 + \frac{a_8}{r^2}\right) \frac{d^2 u^s(r)}{dr^2} + \left(\frac{a_5}{r} - \frac{a_6}{r^3}\right) \frac{du^b(r)}{dr} + \left(\frac{a_7}{r} - \frac{a_8}{r^3}\right) \frac{du^s(r)}{dr} \\ &+ \left(a_9 + \frac{a_{10}}{r^2} + \frac{a_{11}}{r^4}\right) u^b(r) + \left(a_9 + \frac{a_{12}}{r^2} + \frac{a_{13}}{r^4}\right) u^s(r) = 0, \end{aligned} \quad (22)$$

$$\begin{aligned} &b_1 \frac{d^4 u^b(r)}{dr^4} + b_2 \frac{d^4 u^s(r)}{dr^4} + \frac{b_3}{r} \frac{d^3 u^b(r)}{dr^3} + \frac{b_4}{r} \frac{d^3 u^s(r)}{dr^3} + \left(b_5 + \frac{b_6}{r^2}\right) \frac{d^2 u^b(r)}{dr^2} \\ &+ \left(b_7 + \frac{b_8}{r^2}\right) \frac{d^2 u^s(r)}{dr^2} + \left(\frac{b_5}{r} - \frac{b_6}{r^3}\right) \frac{du^b(r)}{dr} + \left(\frac{b_7}{r} - \frac{b_8}{r^3}\right) \frac{du^s(r)}{dr} \\ &+ \left(b_9 + \frac{b_{10}}{r^2} + \frac{b_{11}}{r^4}\right) u^b(r) + \left(b_9 + \frac{b_{12}}{r^2} + \frac{b_{13}}{r^4}\right) u^s(r) = 0, \end{aligned} \quad (23)$$

where

$$\begin{aligned} \{a_1, a_2, a_3, a_4\} &= \{-k_1, -k_2, 2a_1, 2a_2\}, & \{b_1, b_2, b_3, b_4\} &= \{a_2, -k_4, a_4, 2b_2\}, \\ a_5 &= -I_1 \omega^2 + N^T + N^C + J_2, & b_5 &= a_7, \\ a_6 &= 2k_7 \mu_n^2 + 2\bar{k}_1 \mu_n^2 + k_1, & b_6 &= a_8, \\ a_7 &= -I_2 \omega^2 + N^T + N^C + J_2, & b_7 &= -I_3 \omega^2 + N^T + N^C + J_2 + k_6, \\ a_8 &= 2k_8 \mu_n^2 + 2\bar{k}_2 \mu_n^2 + k_2, & b_8 &= 2k_9 \mu_n^2 + 2\bar{k}_4 \mu_n^2 + k_4, \\ a_9 &= I_4 \omega^2 - J_1, & b_9 &= a_9, \\ a_{10} &= I_1 \mu_n^2 \omega^2 - (N^T + N^C) \mu_n^2 - J_2 \mu_n^2, & b_{10} &= a_{12}, \\ a_{11} &= -k_1 \mu_n^4 + 2k_1 \mu_n^2 + 2k_7 \mu_n^2 + 2\bar{k}_1 \mu_n^2, & b_{11} &= a_{13}, \\ a_{12} &= I_2 \mu_n^2 \omega^2 - (N^T + N^C) \mu_n^2 - J_2 \mu_n^2, & b_{12} &= I_3 \mu_n^2 \omega^2 - (N^T + N^C) \mu_n^2 - J_2 \mu_n^2 - k_6 \mu_n^2, \\ a_{13} &= -k_2 \mu_n^4 + 2k_2 \mu_n^2 + 2k_8 \mu_n^2 + 2\bar{k}_2 \mu_n^2, & b_{13} &= -k_4 \mu_n^4 + 2k_4 \mu_n^2 + 2k_9 \mu_n^2 + 2\bar{k}_4 \mu_n^2. \end{aligned} \quad (24)$$

In the current study, the edge of the organic solar cell ( $r = R$ ) is assumed to be clamped. Therefore, we have

$$u^b = u^s = 0. \quad (25)$$

Additionally, the conditions at the center of the solid circular cell ( $r = 0$ ) are shown as [24,25]

$$\frac{du^b}{dr} = \frac{du^s}{dr} = 0. \quad (26)$$

#### 4. Solution Methods

This section uses the DQM, which is used along the radial direction, to solve the motion Equations (22) and (23). Many researchers have used the DQM extensively to solve the governing equations of structures [26–28]. This is because it provides simple formulations and requires less computational effort than other numerical techniques. The current circular cell is discretized by  $n$  grid points in domain ( $0 \leq r \leq R$ ). The displacement derivatives are roughly represented as a weighted linear sum of function values at each discrete position in accordance with the DQM as [29]

$$\begin{aligned} \frac{d^q u^b}{dr^q} &= \sum_{j=1}^n C_{ij}^{(q)} u_j^b, \\ \frac{d^q u^s}{dr^q} &= \sum_{j=1}^n C_{ij}^{(q)} u_j^s, \quad i = 1, 2, \dots, n, \end{aligned} \quad (27)$$

where  $u_i^b = u^b(r_i)$  and  $u_i^s = u^s(r_i)$ , while the weighting coefficients for the  $q$ th-order derivative are represented by  $C_{ij}^{(q)}$ . These are given as [29]

$$\begin{aligned} C_{ij}^{(1)} &= \frac{K(r_i)}{(r_i - r_j)K(r_j)}, \quad i, j = 1, 2, \dots, n, \quad i \neq j, \\ C_{ii}^{(1)} &= -\sum_{i=1}^n C_{li}^{(1)}, \quad i = 1, 2, \dots, n, \quad i \neq l, \\ K(r_i) &= \prod_{i=1}^n (r_i - r_j), \quad i \neq j, \end{aligned} \quad (28)$$

Moreover, weighting coefficients  $C_{ij}^{(q)}$  ( $q > 1$ ) for the higher-order derivatives are computed as follows [29]:

$$C_{ij}^{(q)} = \sum_{l=1}^n C_{il}^{(1)} C_{lj}^{(q-1)}, \quad i, j = 1, 2, \dots, n. \quad (29)$$

Additionally, the mesh points  $r_i$  are estimated using the Gauss–Chebyshev–Lobatto technique as [29]

$$r_i = \frac{R}{2} \left[ 1 - \cos\left(\pi \frac{i-1}{n-1}\right) \right]. \quad (30)$$

The governing equations can be discretized by applying Equation (27) to Equations (22) and (23) as follows:

$$\begin{aligned} &a_1 \sum_{j=1}^n C_{ij}^{(4)} u_j^b + a_2 \sum_{j=1}^n C_{ij}^{(4)} u_j^s + \frac{a_3}{r_i} \sum_{j=1}^n C_{ij}^{(3)} u_j^b + \frac{a_4}{r_i} \sum_{j=1}^n C_{ij}^{(3)} u_j^s + \left( a_5 + \frac{a_6}{r_i^2} \right) \sum_{j=1}^n C_{ij}^{(2)} u_j^b \\ &+ \left( a_7 + \frac{a_8}{r_i^2} \right) \sum_{j=1}^n C_{ij}^{(2)} u_j^s + \left( \frac{a_5}{r_i} - \frac{a_6}{r_i^3} \right) \sum_{j=1}^n C_{ij}^{(1)} u_j^b + \left( \frac{a_7}{r_i} - \frac{a_8}{r_i^3} \right) \sum_{j=1}^n C_{ij}^{(1)} u_j^s \\ &+ \left( a_9 + \frac{a_{10}}{r_i^2} + \frac{a_{11}}{r_i^4} \right) u_j^b(r) + \left( a_9 + \frac{a_{12}}{r_i^2} + \frac{a_{13}}{r_i^4} \right) u_j^s(r) = 0, \end{aligned} \quad (31)$$

$$\begin{aligned}
& b_1 \sum_{j=1}^n C_{ij}^{(4)} u_j^b + b_2 \sum_{j=1}^n C_{ij}^{(4)} u_j^s + \frac{b_3}{r_i} \sum_{j=1}^n C_{ij}^{(3)} u_j^b + \frac{b_4}{r_i} \sum_{j=1}^n C_{ij}^{(3)} u_j^s + \left( b_5 + \frac{b_6}{r_i^2} \right) \sum_{j=1}^n C_{ij}^{(2)} u_j^b \\
& + \left( b_7 + \frac{b_8}{r_i^2} \right) \sum_{j=1}^n C_{ij}^{(2)} u_j^s + \left( \frac{b_5}{r_i} - \frac{b_6}{r_i^3} \right) \sum_{j=1}^n C_{ij}^{(1)} u_j^b + \left( \frac{b_7}{r_i} - \frac{b_8}{r_i^3} \right) \sum_{j=1}^n C_{ij}^{(1)} u_j^s \\
& + \left( b_9 + \frac{b_{10}}{r_i^2} + \frac{b_{11}}{r_i^4} \right) u_j^b(r) + \left( b_9 + \frac{b_{12}}{r_i^2} + \frac{b_{13}}{r_i^4} \right) u_j^s(r) = 0, \quad i = 2 \dots (n-1).
\end{aligned} \tag{32}$$

Additionally, the discretization form of the boundary conditions can be expressed as follows:

$$\begin{aligned}
& u_i^b = u_i^s = 0, \quad \text{at } r = R, \\
& \sum_{j=1}^n C_{ij}^{(1)} u_j^b = \sum_{j=1}^n C_{ij}^{(1)} u_j^s = 0, \quad \text{at } r = 0, \quad i = 1, n.
\end{aligned} \tag{33}$$

Equations (31) and (32) represent an eigenvalue problem. By solving this problem with Boundary conditions (33), we can obtain the lowest eigenfrequency  $\omega$ .

## 5. Numerical Results

In order to examine the effects of various factors on the vibration of circular organic solar cells exposed to hygrothermal conditions sitting on an elastic basis, we present here a number of numerical examples. The following data are used (unless otherwise stated):  $R/h = 10$ ,  $\hat{J}_1 = 15$ ,  $\hat{J}_2 = 100$ ,  $T = 150$  K,  $C = 1.5\%$ . The current analysis uses the following dimensionless values:

$$\omega^* = 100h\omega \sqrt{\frac{\rho^{(1)}}{E^{(1)}}}, \quad \hat{J}_1 = \frac{R^4 J_1}{D^{(1)}}, \quad \hat{J}_2 = \frac{R^2 J_2}{D^{(1)}}, \quad D^{(1)} = \frac{h^3 E^{(1)}}{12(1 - [\nu^{(1)}]^2)}. \tag{34}$$

The thickness and properties of each layer are provided in Table 1.

**Table 1.** Thickness and properties of the cell layers [15].

Layer	Material	Thickness (m)	$E$ (GPa)	$\nu$	$\rho$ (g/cm <sup>3</sup> )	$\alpha$ (K <sup>-1</sup> )	$\beta$ (wt.%H <sub>2</sub> O) <sup>-1</sup>
5	Glass	$0.55 \times 10^{-3}$	69	0.23	2.4	$9 \times 10^{-6}$	0.014
4	ITO	$0.12 \times 10^{-6}$	116	0.35	7.12	$6 \times 10^{-6}$	0.002
3	PEDOT:PSS	$0.5 \times 10^{-7}$	2.3	0.4	1	$70 \times 10^{-6}$	0.07
2	P3HT:PCBM	$0.17 \times 10^{-6}$	6	0.23	1.2	$120 \times 10^{-6}$	0.9
1	Aluminum	$0.1 \times 10^{-6}$	70	0.35	2.601	$23 \times 10^{-6}$	0.44

It is necessary to ascertain the minimum number of discrete points for the DQM's convergent solution. As a result, a convergence analysis of the DQM for circular organic solar cells sitting on elastic foundations is shown in Table 2. It is seen that the findings converge around 15 grid points.

**Table 2.** DQM convergence analysis for fundamental frequency  $\omega^*$  of circular organic solar cells for various temperatures.

$n$	$\omega^*$					
	$\Delta T = 0$ K	$\Delta T = 100$ K	$\Delta T = 200$ K	$\Delta T = 300$ K	$\Delta T = 400$ K	$\Delta T = 500$ K
9	1.30054	1.29443	1.28828	1.29443	1.27584	1.26955
11	1.73167	1.72709	1.72251	1.72709	1.71329	1.70867
13	1.95136	1.94668	1.94200	1.94668	1.93259	1.92788
15	2.05020	2.04445	2.03869	2.04445	2.02707	2.02122
17	2.05268	2.04396	2.03513	2.04396	2.01712	2.00793

In order to confirm the accuracy of the proposed theory, the fundamental frequency  $\omega^*$  of clamped organic solar cells obtained by the present theory is compared with that obtained by the TDPT [18], the SDPT [19], the HDPT [20], and the EDPT [21] for various values of the radius-to-thickness ratio  $R/h$ , as indicated in Table 3. The present theory predicts results in excellent agreement with the results of other higher-order shear deformation theories, especially for large values of the ratio  $R/h$ . Further, it is clear that with increasing the radius-to-thickness ratio  $R/h$ , the cells become weaker, so the eigenfrequency decreases as ratio  $R/h$  increases. In addition, it should be noted that as the circular solar cell expands, the humidity reduces the effect of the temperature on the cells.

**Table 3.** Comparing the fundamental frequency  $\omega^*$  of circular organic solar cells with simple support.

Theory	Theory	$\omega^*$					
		$R/h = 10$	$R/h = 15$	$R/h = 20$	$R/h = 25$	$R/h = 30$	$R/h = 35$
Hygrothermal	TDPT [18]	4.914390	0.435898	0.223034	0.205136	0.181341	0.151995
	SDPT [19]	4.920000	0.435888	0.223039	0.205133	0.181344	0.151997
	HDPT [20]	4.914060	0.435898	0.223034	0.205136	0.181341	0.151995
	EDPT [21]	4.935520	0.435858	0.223054	0.205122	0.181354	0.152001
	Present	4.917470	0.435894	0.223037	0.205135	0.181342	0.151996
Thermal	TDPT [18]	5.024970	0.704606	0.323740	0.179265	0.108809	0.072579
	SDPT [19]	5.028610	0.704371	0.323709	0.179259	0.108809	0.072580
	HDPT [20]	5.024710	0.704600	0.323740	0.179265	0.108809	0.072579
	EDPT [21]	5.038180	0.703559	0.323607	0.179239	0.108806	0.072581
	Present	5.027050	0.704516	0.323727	0.179262	0.108809	0.072579

Tables 4–6 display the effects of the temperature and moisture changes ( $\Delta T$ ,  $\Delta C$ ) on the fundamental frequency  $\omega^*$  of the circular organic solar cells under uniform (Table 4), linear (Table 5), nonlinear (Table 6) hygrothermal distributions through the thickness. Also, the effects of the thickness-to-radius ratios  $R/h$  is taken into consideration. As mentioned above, we see that the result values decrease with increasing radius. Regardless of the hygrothermal distribution type, the increase in the moisture change has a negative effect on the vibration of cells with small radius, while it has a positive effect on the cells that have a large radius. For large cells ( $R/h = 30$ ), as the temperature increases, the cell stiffness reduces, so vibration decreases, while this sense is reversed when the moisture is included because the humidity reduces the effect of the temperature on the expanded cells ( $R/h = 30$ ).

To explain the influences of the uniform, linear, and nonlinear temperature and moisture changes ( $\Delta T$ ,  $\Delta C$ ) on the fundamental frequency  $\omega^*$  in graphical form, Figure 2 is presented ( $R/h = 10$ ). Since the increment in the humidity and temperature leads to a weakening of structures, the frequency of the circular organic solar cells decreases as the temperature and moisture increase.

**Table 4.** The fundamental frequency  $\omega^*$  of a circular organic solar cell under uniform hydrothermal rise.

$R/h$	$\Delta C(\%)$	$\omega^*$					
		$\Delta T = 0 \text{ K}$	$\Delta T = 100 \text{ K}$	$\Delta T = 200 \text{ K}$	$\Delta T = 300 \text{ K}$	$\Delta T = 400 \text{ K}$	$\Delta T = 500 \text{ K}$
10	0	5.06359	5.05314	5.04280	5.03257	5.02244	5.01243
	1	4.91207	4.90327	4.89457	4.88598	4.87748	4.86908
	2	1.08622	1.05971	1.03495	1.01181	0.99018	0.97000
	3	0.83459	0.82893	0.82442	0.82105	0.81880	0.81767
	4	0.86837	0.87825	0.88885	0.90013	0.91206	0.92460
	5	1.08499	1.10139	1.11783	1.13424	1.15056	1.16674
20	0	0.40882	0.38455	0.36136	0.33937	0.31870	0.29946
	1	0.22459	0.23185	0.24100	0.25170	0.26362	0.27643
	2	0.38907	0.39328	0.39694	0.40036	0.40380	0.40746
	3	0.43876	1.59023	0.54061	0.51228	0.51028	0.51255
	4	0.56135	0.56569	0.56988	0.57386	0.57759	0.58097
	5	0.65593	0.65689	0.65894	0.66160	0.66463	0.66790
30	0	0.16871	0.15026	0.13299	0.11795	0.10627	0.09909
	1	0.18233	0.18605	0.19014	0.19480	0.19986	0.20491
	2	0.26686	0.27101	0.27488	0.27832	0.28089	0.28106
	3	0.33597	0.33948	0.34296	0.34641	0.34983	0.35319
	4	0.83529	0.41018	0.40642	0.40695	0.40871	0.41098
	5	0.44066	0.44349	0.44630	0.44910	0.45188	0.45466

**Table 5.** The fundamental frequency  $\omega^*$  of a circular organic solar cell under linear hydrothermal rise.

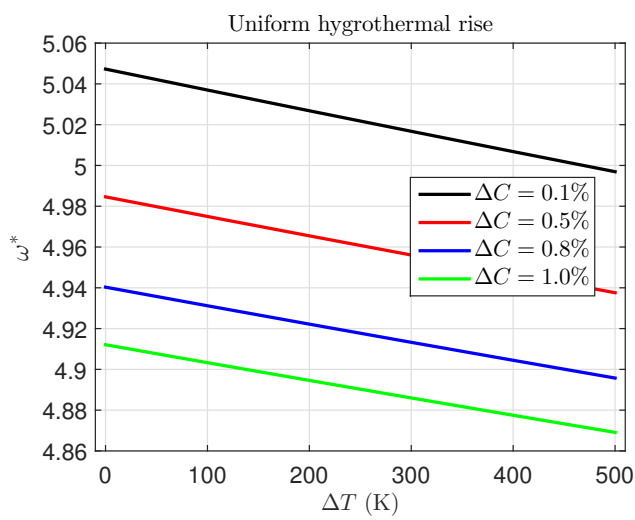
$R/h$	$\Delta C(\%)$	$\omega^*$					
		$\Delta T = 0 \text{ K}$	$\Delta T = 100 \text{ K}$	$\Delta T = 200 \text{ K}$	$\Delta T = 300 \text{ K}$	$\Delta T = 400 \text{ K}$	$\Delta T = 500 \text{ K}$
10	0	5.03257	5.02749	5.02245	5.01743	5.01244	5.00747
	1	4.95666	4.95200	4.94736	4.94275	4.93817	4.93361
	2	4.88704	4.88278	4.87854	4.87433	4.87014	1.61646
	3	1.25400	1.23394	1.21481	1.19652	1.17900	1.16218
	4	1.01745	1.00627	0.99546	0.98502	0.97494	0.96520
	5	0.88241	0.87638	0.87065	0.86522	0.86009	0.85526
20	0	0.33937	0.32886	0.31870	0.30890	0.29947	0.290432
	1	0.22434	0.22144	0.21920	0.21764	0.21677	0.21657
	2	0.25029	0.25604	0.26207	0.26833	0.27478	0.28138
	3	0.35001	0.35546	0.36058	0.36535	0.36976	0.37381
	4	0.39951	0.40121	0.40292	0.40469	0.40651	0.40841
	5	0.43303	0.43555	0.43801	0.44039	0.44263	0.44466
30	0	0.11795	0.11162	0.10627	0.10206	0.09910	0.09749
	1	0.14296	0.14931	0.15529	0.16078	0.16565	0.16985
	2	0.19419	0.19666	0.19921	0.20178	0.20430	0.20665
	3	0.24398	0.24626	0.24858	0.25092	0.25326	0.25558
	4	0.27752	0.27907	0.28037	0.28128	0.28146	0.28007
	5	0.31861	0.32011	0.32169	0.32333	0.32501	0.32672

**Table 6.** The fundamental frequency  $\omega^*$  of a circular organic solar cell under nonlinear hydrothermal rise.

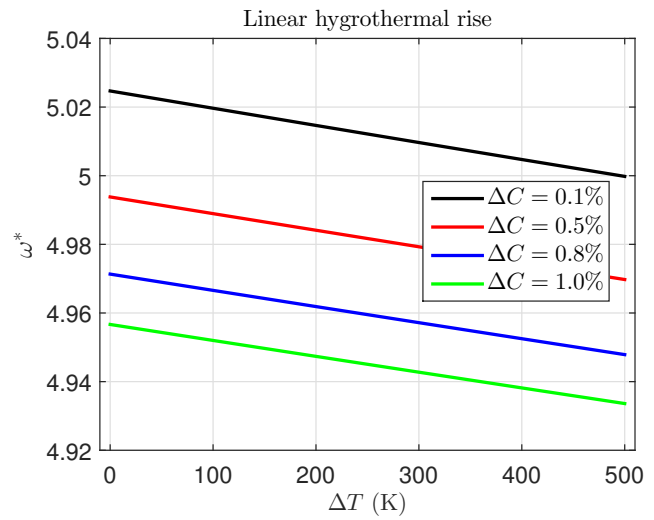
$R/h$	$\Delta C(\%)$	$\omega^*$					
		$\Delta T = 0 \text{ K}$	$\Delta T = 100 \text{ K}$	$\Delta T = 200 \text{ K}$	$\Delta T = 300 \text{ K}$	$\Delta T = 400 \text{ K}$	$\Delta T = 500 \text{ K}$
10	0	5.03257	5.02888	5.02520	5.02154	5.01789	5.01426
	1	4.97677	4.97329	4.96984	4.96639	4.96296	4.95955
	2	4.92432	4.92106	4.91782	4.91458	4.91137	4.90816
	3	4.87515	4.87210	4.86906	1.61790	1.56341	1.52307
	4	1.28489	1.26907	1.25384	1.23917	1.22501	1.21132
	5	1.08890	1.07899	1.06933	1.05991	1.05071	1.04174

Table 6. Cont.

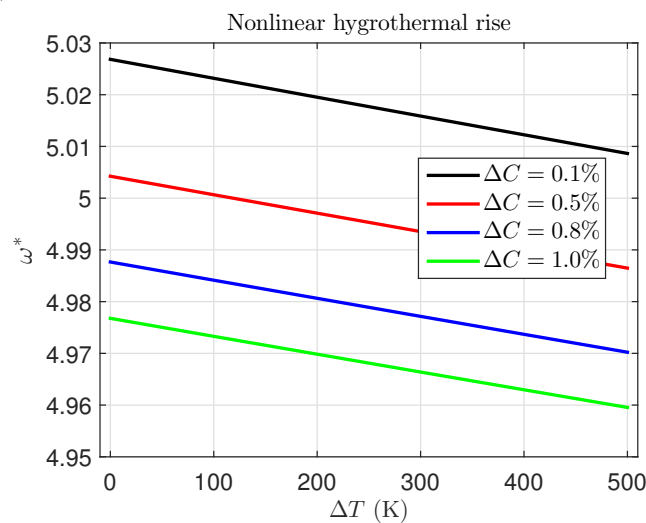
R/h	$\Delta C(\%)$	$\omega^*$					
		$\Delta T = 0$ K	$\Delta T = 100$ K	$\Delta T = 200$ K	$\Delta T = 300$ K	$\Delta T = 400$ K	$\Delta T = 500$ K
20	0	0.33937	0.33170	0.32421	0.31691	0.30980	0.30288
	1	0.24372	0.23964	0.23587	0.23240	0.22926	0.22645
	2	0.21824	0.21948	0.22104	0.22292	0.22509	0.22755
	3	0.26709	0.27173	0.27647	0.28128	0.28615	0.29106
	4	0.34161	0.34590	0.35005	0.35404	0.35786	0.36150
	5	0.38862	0.39027	0.39181	0.39326	0.39463	0.39595
30	0	0.11795	0.11325	0.10906	0.10542	0.10240	0.10003
	1	0.11585	0.12017	0.12471	0.12940	0.13416	0.13895
	2	0.17643	0.17822	0.17981	0.18126	0.18263	0.18397
	3	0.20128	0.20313	0.20493	0.20662	0.20813	0.20930
	4	0.24090	0.24240	0.24400	0.24565	0.24733	0.24902
	5	0.26644	0.26798	0.26949	0.27098	0.27242	0.27383



(a)



(b)



(c)

Figure 2. Effects of temperature and moisture on the fundamental frequency  $\omega^*$  of a circular organic solar cell under (a) uniform hygrothermal rise, (b) linear hygrothermal rise, and (c) nonlinear hygrothermal rise.

Table 7 shows how the fundamental frequency  $\omega^*$  of circular organic solar cells is affected by the elastic foundation stiffness ( $\hat{f}_1, \hat{f}_2$ ). It is evident that when the shear elastic foundation coefficient  $\hat{f}_2$  rises, the fundamental frequency rises as well. When the shear foundation is not considered, the increase in the Winkler foundation coefficient leads to an increment in the vibration, while this is reversed with the presence of the shear layer. It should also be noted that the effects of the elastic foundation coefficient on the vibration are more pronounced for the hygrothermal load. In general, the presence of Winkler or shear elastic foundation boosts the cell strength; therefore, the frequencies increase when considering the elastic foundations.

**Table 7.** Fundamental frequency  $\omega^*$  of different kinds of circular organic solar cells with varying foundation stiffness values in thermal and hygrothermal environments.

Load	$\hat{f}_2$	$\omega^*$					
		$\hat{f}_1 = 0$	$\hat{f}_1 = 200$	$\hat{f}_1 = 400$	$\hat{f}_1 = 600$	$\hat{f}_1 = 800$	$\hat{f}_1 = 1000$
$\Delta T = \Delta C = 0$	0	4.94110	4.94279	4.94429	4.94561	4.94678	4.94779
	20	5.10778	5.10778	5.10766	5.10742	5.10708	5.10663
	40	5.30476	5.30335	5.30187	5.30031	5.29869	5.29699
	60	5.53539	5.53280	5.53016	5.52748	5.52474	5.52196
	80	5.80475	5.80113	5.79747	5.79377	5.79005	5.78630
	100	6.12064	6.11605	6.11143	6.10679	6.10213	6.09745
Thermal ( $\Delta T = 200$ K $\Delta C = 0\%$ )	0	4.90736	4.90946	4.91137	4.91309	4.91463	4.91600
	20	5.06754	5.06789	5.06810	5.06820	5.06818	5.06804
	40	5.25741	5.25630	5.25510	5.25383	5.25247	5.25105
	60	5.48006	5.47773	5.47533	5.47289	5.47039	5.46785
	80	5.74010	5.73670	5.73326	5.72979	5.72629	5.72275
	100	6.04458	6.04021	6.03580	6.03138	6.02693	6.02246
Hygrothermal ( $\Delta T = 200$ K $\Delta C = 2\%$ )	0	1.26959	1.15219	1.01976	0.86528	0.67357	0.39326
	20	4.95464	4.95616	4.95750	4.95868	4.95970	4.96057
	40	5.12388	5.12374	5.12349	5.12313	5.12266	5.12210
	60	5.32366	5.32214	5.32055	5.31889	5.31716	5.31536
	80	5.55748	5.55479	5.55206	5.54928	5.54645	5.54358
	100	5.83057	5.82685	5.82311	5.81933	5.81552	5.81169

## 6. Conclusions

In this work, the free vibration of circular organic solar cells resting on an elastic foundation and exposed to temperature and moisture conditions is analyzed for the first time. Within the framework of a new inverse hyperbolic two-variable shear deformation plate theory, the displacement field is modeled. Accordingly, two equations of motion are developed employing Hamilton's principle. These equations are homogeneous with variable coefficients. It is difficult to solve this system analytically, so the differential quadrature method is utilized here to deal with it numerically. In order to verify the correctness of the suggested theory, the current findings are compared with those documented by other higher-order theories. In addition, the impacts of different parameters, including geometrical configuration, elastic foundation parameters, temperature, and moisture concentration, on the vibration of the circular organic solar cells are discussed. It can be concluded that the eigenfrequency reduces as the radius of the cell increases. For a small cell radius, the increment in the temperature and humidity leads to a noticeable reduction in the eigenfrequency, while this behavior is reversed for a large radius. As expected, the elastic foundation enhances the organic cells, so the eigenfrequency increases as the foundation parameters increase.

**Author Contributions:** Conceptualization, M.A., M.A.A. and M.S.; methodology, M.A., M.A.A. and M.S.; software, M.S.; validation, M.S.; formal analysis, M.A., M.A.A. and M.S.; investigation, M.A., M.A.A. and M.S.; resources, M.A., M.A.A. and M.S.; data curation, M.A., M.A.A. and M.S.; writing—original draft preparation, M.A., M.A.A. and M.S.; writing—review and editing, M.A., M.A.A. and M.S.; visualization, M.A., M.A.A. and M.S.; supervision, M.S.; project administration, M.A., M.A.A. and M.S.; funding acquisition, M.A., M.A.A. and M.S. All authors have read and agreed to the published version of the manuscript.

**Funding:** This work was supported by the Deanship of Scientific Research, Vice Presidency for Graduate Studies and Scientific Research, King Faisal University, Saudi Arabia (grant No. GrantA082).

**Institutional Review Board Statement:** Not applicable.

**Informed Consent Statement:** Not applicable.

**Data Availability Statement:** Data are contained within the article.

**Conflicts of Interest:** The authors declare no conflicts of interest.

## References

1. Abazid, M.A.; Lakhal, A.; Louis, A.K. A stable numerical algorithm for the design of anti-reflection coating for solar cells. *Int. J. Renew. Energy Technol.* **2016**, *7*, 97–111. [[CrossRef](#)]
2. Hoppe, H.; Sariciftci, N.S. Organic solar cells: An overview. *J. Mater. Res.* **2004**, *19*, 1924–1945. [[CrossRef](#)]
3. Brabec, C.J. Organic photovoltaics: Technology and market. *Sol. Energy Mater. Sol. Cells* **2004**, *83*, 273–292. [[CrossRef](#)]
4. Liu, S.; Wang, K.; Wang, B.; Li, J.; Zhang, C. Sunlight irradiation and wind effect on the interlaminar stresses of the organic solar cell. *Arch. Appl. Mech.* **2021**, *91*, 3203–3221. [[CrossRef](#)]
5. Joodaki, M.; Salari, M. Investigation of the tensile strain influence on flicker noise of organic solar cells under dark condition. *Org. Electron.* **2018**, *59*, 230–235. [[CrossRef](#)]
6. Duc, N.D.; Seung-Eock, K.; Quan, T.Q.; Long, D.D.; Anh, V.M. Nonlinear dynamic response and vibration of nanocomposite multilayer organic solar cell. *Compos. Struct.* **2018**, *184*, 1137–1144. [[CrossRef](#)]
7. Zhang, Y.; Zhuang, X.; Zhou, K.; Cai, C.; Hu, Z.; Zhang, J.; Zhu, Y. Vibration treated carbon electrode for highly efficient hole-conductor-free perovskite solar cells. *Org. Electron.* **2018**, *52*, 159–164. [[CrossRef](#)]
8. Liao, H.; Deng, Q.; Shen, Y.; Wang, G.; Wang, S.; Mao, Y. Theoretical analysis of doping concentration, layer thickness and barrier height effects on BaSi<sub>2</sub> based homojunction solar cells toward high efficiency. *Sol. Energy* **2020**, *201*, 857–865. [[CrossRef](#)]
9. Dat, N.D.; Anh, V.M.; Quan, T.Q.; Duc, P.T.; Duc, N.D. Nonlinear stability and optimization of thin nanocomposite multilayer organic solar cell using Bees Algorithm. *Thin-Walled Struct.* **2020**, *149*, 106520. [[CrossRef](#)]
10. Van Tuyen, B. Buckling and free vibration response of organic nanobeams taking the temperature into account. *Ain Shams Eng. J.* **2023**, *14*, 102193. [[CrossRef](#)]
11. Liu, S.; Wang, K.; Wang, B.; Li, J.; Zhang, C. Size effect on thermo-mechanical instability of micro/nano scale organic solar cells. *Meccanica* **2022**, *57*, 87–107. [[CrossRef](#)]
12. Tien, D.M.; Thom, D.V.; Minh, P.V.; Tho, N.C.; Doan, T.N.; Mai, D.N. The application of the nonlocal theory and various shear strain theories for bending and free vibration analysis of organic nanoplates. *Mech. Based Des. Struct. Mach.* **2023**, *52*, 588–610. [[CrossRef](#)]
13. Li, Q.; Wu, D.; Gao, W.; Tin-Loi, F. Size-dependent instability of organic solar cell resting on Winkler–Pasternak elastic foundation based on the modified strain gradient theory. *Int. J. Mech. Sci.* **2020**, *177*, 105306. [[CrossRef](#)]
14. Li, Q.; Wu, D.; Gao, W.; Tin-Loi, F.; Liu, Z.; Cheng, J. Static bending and free vibration of organic solar cell resting on Winkler–Pasternak elastic foundation through the modified strain gradient theory. *Eur. J. Mech.-A/Solids* **2019**, *78*, 103852. [[CrossRef](#)]
15. Li, Q.; Wang, Q.; Wu, D.; Chen, X.; Yu, Y.; Gao, W. Geometrically nonlinear dynamic analysis of organic solar cell resting on Winkler–Pasternak elastic foundation under thermal environment. *Compos. Part B Eng.* **2019**, *163*, 121–129. [[CrossRef](#)]
16. Van Quyen, N.; Duc, N.D. Vibration and nonlinear dynamic response of nanocomposite multi-layer solar panel resting on elastic foundations. *Thin-Walled Struct.* **2022**, *177*, 109412. [[CrossRef](#)]
17. Shimpi, R.P. Refined plate theory and its variants. *AIAA J.* **2002**, *40*, 137–146. [[CrossRef](#)]
18. Reddy, J.N. A simple higher-order theory for laminated composite plates. *J. Appl. Mech.* **1984**, *51*, 745–752. [[CrossRef](#)]
19. Touratier, M. An efficient standard plate theory. *Int. J. Eng. Sci.* **1991**, *29*, 901–916. [[CrossRef](#)]
20. Soldatos, K. A transverse shear deformation theory for homogeneous monoclinic plates. *Acta Mech.* **1992**, *94*, 195–220. [[CrossRef](#)]
21. Karama, M.; Afaq, K.; Mistou, S. Mechanical behaviour of laminated composite beam by the new multi-layered laminated composite structures model with transverse shear stress continuity. *Int. J. Solids Struct.* **2003**, *40*, 1525–1546. [[CrossRef](#)]
22. Reddy, J.N. *Energy Principles and Variational Methods in Applied Mechanics*; John Wiley & Sons: Hoboken, NJ, USA, 2017.
23. Sobhy, M.; Alakel Abazid, M. Mechanical and thermal buckling of FG-GPLs sandwich plates with negative Poisson’s ratio honeycomb core on an elastic substrate. *Eur. Phys. J. Plus* **2022**, *137*, 1–21. [[CrossRef](#)]

24. Safarpour, M.; Rahimi, A.; Alibeigloo, A.; Bisheh, H.; Forooghi, A. Parametric study of three-dimensional bending and frequency of FG-GPLRC porous circular and annular plates on different boundary conditions. *Mech. Based Des. Struct. Mach.* **2021**, *49*, 707–737. [[CrossRef](#)]
25. Sobhy, M. 3-D elasticity numerical solution for magneto-hydrothermal bending of FG graphene/metal circular and annular plates on an elastic medium. *Eur. J. Mech.-A/Solids* **2021**, *88*, 104265. [[CrossRef](#)]
26. Golmakani, M.; Vahabi, H. Nonlocal buckling analysis of functionally graded annular nanoplates in an elastic medium with various boundary conditions. *Microsyst. Technol.* **2017**, *23*, 3613–3628. [[CrossRef](#)]
27. Demir, O.; Balkan, D.; Peker, R.C.; Metin, M.; Arikoglu, A. Vibration analysis of curved composite sandwich beams with viscoelastic core by using differential quadrature method. *J. Sandw. Struct. Mater.* **2020**, *22*, 743–770. [[CrossRef](#)]
28. Sobhy, M. Piezoelectric bending of GPL-reinforced annular and circular sandwich nanoplates with FG porous core integrated with sensor and actuator using DQM. *Arch. Civ. Mech. Eng.* **2021**, *21*, 78. [[CrossRef](#)]
29. Shu, C. *Differential Quadrature and Its Application in Engineering*; Springer Science & Business Media: Berlin/Heidelberg, Germany, 2012.

**Disclaimer/Publisher’s Note:** The statements, opinions and data contained in all publications are solely those of the individual author(s) and contributor(s) and not of MDPI and/or the editor(s). MDPI and/or the editor(s) disclaim responsibility for any injury to people or property resulting from any ideas, methods, instructions or products referred to in the content.